Model for friction and wear reduction through piezoelectrically-assisted ultrasonic lubrication

Sheng Dong, Marcelo J. Dapino

Smart Vehicle Concepts Center, Department of Mechanical and Aerospace Engineering,
The Ohio State University, Columbus, OH 43210, USA

ABSTRACT

This article presents an analytical model for piezoelectrically-assisted ultrasonic friction and wear reduction. A cube is employed to represent the asperities in contact between two surfaces. Dynamic friction is considered as the sum of two friction components that depend on deformation of the cube and relative velocity. Ultrasonic vibrations change the geometry, contact stiffness, and deformation of the cube, as well as the relative velocity, which leads to a reduction in the effective dynamic friction. Volume loss of surface wear is explained by the integral of half of the cube volume over the time duration of the sliding. Change of the cube geometry caused by ultrasonic vibrations results in a change of the cube volume. A piezoelectrically-assisted tribometer was designed and built for pin-on-disc friction and wear tests. The experimental measurements validate the model for ultrasonic friction reduction at various macroscopic sliding velocities, and for ultrasonic wear reduction at various sliding distances with most errors less than 10%.

Keywords: Analytical "cube" model, ultrasonic lubrication, piezoelectric actuator, friction reduction, wear reduction

1. INTRODUCTION

Friction is the resistance to the relative motion between two surfaces in contact. Abrasive wear, the removal of materials at the contact surface due to plastic deformation and breakage of asperities, takes place in concert with friction.[1] By superimposing ultrasonic vibrations onto the macroscopic velocity, friction and abrasive wear can be reduced.

Bharadwaj and Dapino[2,3] developed experiments and models in which longitudinal vibrations where used to investigate the effect of macroscopic sliding velocity, normal load, contact stiffness, and global stiffness on friction reduction. Dong and Dapino[4] used the Poisson effect to generate vibrations in combined perpendicular and longitudinal directions relative to the overall sliding direction, and studied the relationship between friction reduction and normal load, contact materials, and global stiffness. Dong and Dapino[5] proposed an analytical "cube" model for ultrasonic friction reduction in which vibrations in three orthogonal directions were implemented.

Dong and Dapino[6] reported experimental measurements on ultrasonic wear reduction conducted between stainless steel and aluminum in a modified tribometer, and determined the effect of linear speed on the degree of wear reduction. The wear reduction data was described using an analytical model based on the "cube" concept developed for friction reduction. The model matches the experimental data with errors less than 15%.[7] This paper proposes improvements to the "cube" model by taking into consideration both the deformation of the asperities and the overall sliding velocity. The model is compared against friction reduction data at different sliding velocities and against wear reduction data collected at different sliding distances conducted on the modified tribometer.

Further author information: (Send correspondence to M.J.D.)
M.J.D.: E-mail: dapino.1@osu.edu, Telephone: 1 614 688 3689
S.D.: E-mail: dong.121@osu.edu, Telephone: 1 614 736 1818

Industrial and Commercial Applications of Smart Structures Technologies 2014,
edited by Kevin M. Farinholt, Steven F. Griffin, Proc. of SPIE Vol. 9059, 90590C
 · doi: 10.1117/12.2046295

2. BACKGROUND

Ultrasonic lubrication has been successfully implemented in practical applications. Piezoelectric materials, the transducer elements that typically drive ultrasonic lubrication systems, have been incorporated into ultrasonic motors smaller than 1 cm^3 and with higher energy density than conventional motors. This makes ultrasonic vibrations of great interests in applications where miniaturized motion control is desired.[8] Acoustic levitation has been studied and utilized as a method to suspend particles. The suspension forces can be increased when the waves reach ultrasonic frequencies along with high energy intensity.[9]

In metal machining and forming processes such as drilling, pressing, sheet rolling, and wire drawing, ultrasonic vibrations have been utilized to reduce the force between tool and workpiece, leading in all cases to improved surface finish.[10] Ultrasonic lubrication is also promising in applications in which traditional lubrication methods are unfeasible (e.g., vehicle seats, space mechanisms) or where friction modulation is desirable (e.g., automotive steering or suspension components).

Ultrasonic vibrations are usually applied only to one of the two contacting surfaces and may be applied in one of three directions relative to the macroscopic sliding velocity: perpendicular, longitudinal or transverse, as shown in Fig. 1. Several studies have been devoted to each of the three directions and combinations thereof. For example, Littman et al.[11,12] used a piezoelectric actuator generating vibrations at 60 kHz, making it slide longitudinally on a guide track. Kumar[13] experimentally determined that longitudinal vibrations were more effective at reducing friction force than transverse vibrations and confirmed that the velocity ratio greatly influences the degree of friction reduction. Popov et al.[14] studied ultrasonic vibrations for different material combinations. It was shown that ultrasonic vibrations create less friction reduction on softer materials than harder ones. They argued that contact stiffness influences the degree of friction force reduction. They proposed an elastic-plastic cube model to explain ultrasonic friction reduction.

There have been attempts at utilizing vibrations to reduce wear between two contacting surfaces. Chowdhury and Helali[15] developed a pin-on-disc test to examine the effects of micro vibration on wear reduction. Vibrations ranging in frequency from dc to 500 Hz were applied normal to the disc surface. They studied the correlation between wear reduction and vibration frequency, relative humidity, and sliding velocity. Their results showed that higher frequency leads to lower wear rates. Bryant and York[16,17] did similar work using high amplitude, low frequency vibrations. They created a slider that vibrates at an amplitude of 10 to 100 μm at frequencies ranging from 10 to 100 Hz, achieving wear reduction of up to 50%.

Goto and Ashida[18,19] conducted tests at frequencies in the ultrasonic range. Applying vibrations normal to the surface of the disc, they studied the relationship between wear rate and normal loads. Their findings show that ultrasonic vibrations can reduce wear under various normal loads. In these tests, the amplitude of the

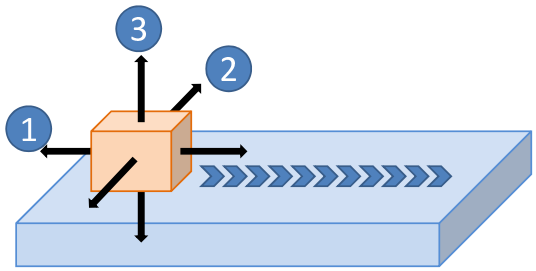

Figure 1. Three possible vibration orientations in ultrasonic lubrication.

ultrasonic vibrations was 8 μm and the normal load was up to 88 N. They also studied the contact time between two surfaces while ultrasonic vibrations were applied.

Littmann et al.[11,12] developed a mathematical relationship between velocity ratio and friction ratio, which indicates that a higher vibration velocity results in a greater friction reduction. Popov et al.[14] presented a relationship between friction reduction and vibration amplitudes under various normal loads. These models were successful in explaining ultrasonic friction reduction with vibrations applied along the sliding direction, but not applicable when the vibrations are perpendicular to the motion. Little modeling work has been conducted on ultrasonic wear reduction. This paper investigates phenomena and conditions not covered in prior work.

3. "CUBE" MODEL

The model is built on the assumption that the contact between two surfaces sliding relative to each other takes place only on the asperities (Fig. 2), which deform elastically and plastically. The height of the asperities is assumed to follow the distribution

$$\phi(z) = ce^{-\lambda z}, \tag{1}$$

where z is the distance between the asperity summit and the mean height of asperities. Here, $c = 17$ and $\lambda = 3$ are parameters used to shape the distribution.[20,21]

A cube is employed to represent the asperities in contact (Fig. 3). The height of the cube d is equal to the distance between the two surfaces in contact. The normal force F_n is the sum of the elastic force F_e and the plastic force F_p, which are functions of d,

$$F_n = F_e + F_p. \tag{2}$$

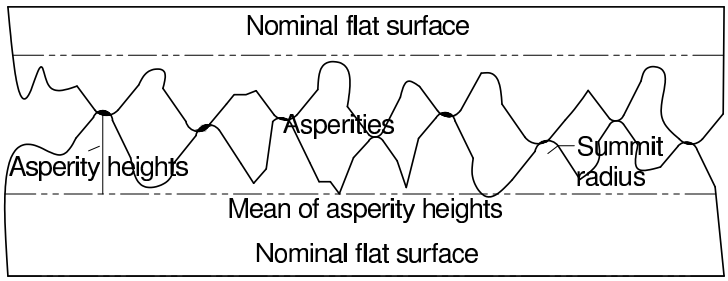

Figure 2. Contacts of asperities between two nominally flat surfaces.

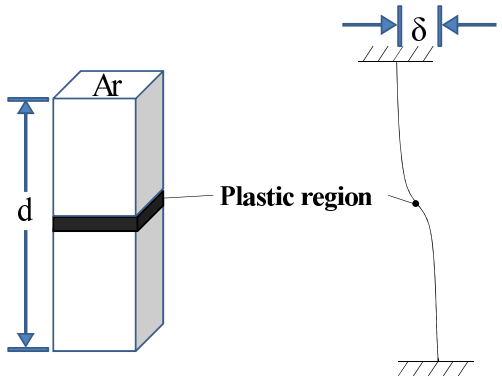

Figure 3. Geometry and deflection of the cube model.

The cube height d corresponding to a normal load F_n is calculated using[5]

$$F_e = \frac{4c\beta A_n E^*(R_q/R_s)^{1/2}}{3\lambda^{5/2}}\Big[\frac{3\sqrt{\pi}}{4}erf\Big(\sqrt{\lambda\omega_c/R_q}\Big) - \frac{(\lambda\omega_c/R_q)^{3/2}+\frac{3}{2}\sqrt{\lambda\omega_c/R_q}}{e^{\lambda\omega_c/R_q}}\Big]e^{-\lambda d/R_q} \quad (3)$$

and

$$F_p = \frac{cA_n\pi\beta C_\nu(1-\nu^2)Y_0}{\lambda^2}\Big(2+\lambda\frac{\omega_c}{R_q}\Big)e^{-\lambda(d+\omega_c)/R_q}, \quad (4)$$

where β is the roughness parameter ($\beta = \eta R_q R_s$), η is the areal density of asperities, A_n is the nominal contact area, R_q is the standard deviation of surface roughness, R_s is the average radius of asperity summits, ν is the Poisson ratio, erf is the error fuction ($\mathrm{erf}(x) = \frac{2}{\sqrt{\pi}}\int_0^x e^{-t^2}dt$), C_ν is a hardness coefficient ($C_\nu = 1.234 + 1.256\nu$), Y_0 is the failure strength of the softer material, and E^* is the combined Young's modulus of the two materials in contact ($1/E^* = (1-\nu_1^2)/E_1 + (1-\nu_2^2)/E_2$). Parameter ω_c is the critical interference, defined as the threshold asperity height separating elastic and plastic deformations, which is calculated as

$$\omega_c = \Big[\frac{C_\nu\pi(1-\nu^2)Y_0}{2E^*}\Big]^2 R_s. \quad (5)$$

The top area of the cube is equal to the actual contact area between the two surfaces:

$$A_r = A_e + A_p, \quad (6)$$

where A_e is the actual contact area of elastically deformed asperities and A_p is that of the plastically deformed asperities. These areas are given by[5]

$$A_e = \frac{c\pi\beta A_n}{\lambda^2}\Big[1-\Big(1+\lambda\frac{\omega_c}{R_q}\Big)e^{\lambda\omega_c/R_q}\Big]e^{-\lambda d/R_q}, \quad (7)$$

and

$$A_p = \frac{c\pi\beta A_n}{\lambda^2}\Big(2+\lambda\frac{\omega_c}{R_q}\Big)e^{-\lambda(d+\omega_c)/R_q}. \quad (8)$$

Therefore, the tangential stiffness of the cube is calculated as

$$K_t = \frac{E^* A_r^2}{d^3}. \quad (9)$$

3.1 Friction reduction model

As illustrated in Fig. 1, ultrasonic vibrations can be decomposed into projections in three orthogonal directions. The displacement components in the three directions are denoted u_1, u_2, and u_3, and the corresponding velocities are $\dot{u_1}$, $\dot{u_2}$, and $\dot{u_3}$.

A simple expression for the relationship between friction force and macroscopic speed is adopted,[22] as shown in Fig. 4. Friction force increases to overcome the static friction F_s, and starts the initial relative sliding with nominal dynamic friction force F_t, which is smaller than the static friction force. As the speed increases, viscous friction F_v becomes significant and the overall friction force F_f increases linearly with increasing macroscopic speed. The overall friction force F_f is considered as the sum of F_t and F_v.

In this paper, it is assumed that nominal dynamic friction F_t is only related to the tangential deformation of the asperities in contact. Hence, the deformation δ is calculated as

$$\delta = F_t/K_t. \quad (10)$$

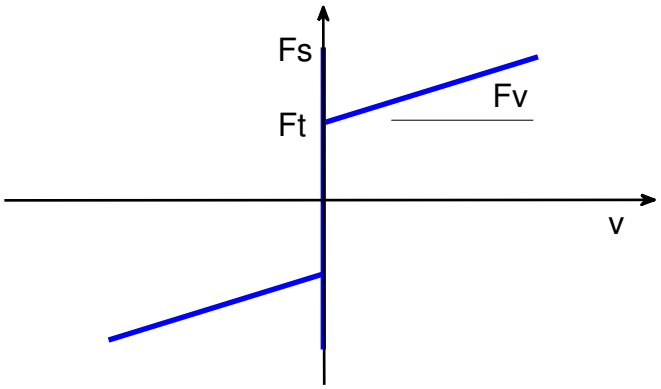

Figure 4. Relationship between friction and velocity.

It is also assumed that the longitudinal projection of the ultrasonic vibrations u_1 is directly added to the deformation. Hence, in the presence of ultrasonic vibrations, a new deformation (denoted δ') is the sum of the initial deformation and the longitudinal projection,

$$\delta' = \delta + u_1. \tag{11}$$

The new cube height (denoted d') is calculated as a direct sum of the initial height and the out-of-plane perpendicular projection u_3,

$$d' = d + u_3. \tag{12}$$

The new actual area of contact changes with the new cube height. It can be calculated using (6)-(8). Therefore, a new tangential stiffness of the cube can be found:

$$K_t{}' = \frac{E^* {A'_r}^2}{{d'}^3}. \tag{13}$$

It is assumed that viscous friction F_v is only dependent on macroscopic velocity. The relationship between viscous friction and relative speed is assumed linear, which is expressed as

$$F_v = \alpha v, \tag{14}$$

where α is the viscous coefficient and v is the relative speed. However, as normal load and relative speed increase, a different relationship may need to be found due to the fact that heat generated at high stress and high speed will change the material properties, which results in non-linear viscous coefficients.

Longitudinal velocity projection $\dot{u_1}$ changes the relative speed to

$$v' = v + \dot{u_1}, \tag{15}$$

which gives a new viscous friction

$$F'_v = \alpha v'. \tag{16}$$

In summary, the friction force when ultrasonic vibrations are applied is calculated as

$$F'_f = F'_t + F'_v. \tag{17}$$

Friction reduction percentage is defined as

$$P_f = \frac{F_f - F'_f}{F_f} \times 100\%. \tag{18}$$

3.2 Wear reduction model

Based on the cube concept, a description for ultrasonic wear reduction is proposed. It can be seen in Fig. 5 that as the top surface moves along the bottom surface, contact asperity pairs deform and break, bringing new asperities into contact. In this study, wear is assumed abrasive, which means that the material of one surface is required to be harder than the material with which it is in contact. Breakage of the contacting asperity pairs is assumed to take place at the roots of the asperities of the softer material. The broken asperities correspond to half of the cube's volume; this removed volume accounts for abrasive wear in the softer material. When ultrasonic vibrations are applied, the contact between the two surfaces is reduced resulting in a reduction of wear.

Over a sliding distance D, the total volume of material removed without ultrasonic vibrations is

$$V = \frac{A_r d}{2}, \tag{19}$$

where V is the volume loss of the aluminum disc, A_r is the actual area of contact between the two surfaces, and d is the height of the cube.

When ultrasonic vibrations are applied, the contact area and the separation between the two surfaces change according to the vibration in the out-of-plane perpendicular direction. As explained previously, we denote A_r' the area of the top of the cube and d' the height of the cube when ultrasonic vibrations are applied. The volume loss of the aluminum disc over the sliding distance D is

$$V' = \frac{1}{2T}\int_0^T A_r' d' dt, \tag{20}$$

where T is the period of ultrasonic vibrations, A_r' is the time-dependent actual area of contact when ultrasonic vibrations are applied, and d' is the time-dependent height of the cube. The wear rate is calculated as

$$W' = \frac{V'}{D} = \frac{1}{2T}\int_0^T \frac{A_r' d'}{D} dt. \tag{21}$$

Wear reduction percentage is calculated as

$$P_w = \frac{W - W'}{W} \times 100\%. \tag{22}$$

For both friction and wear reduction, the modeling error is defined as

$$e = \frac{|\text{test} - \text{model}|}{\text{test}} \times 100\%, \tag{23}$$

which is employed to evaluate the effectiveness of the model.

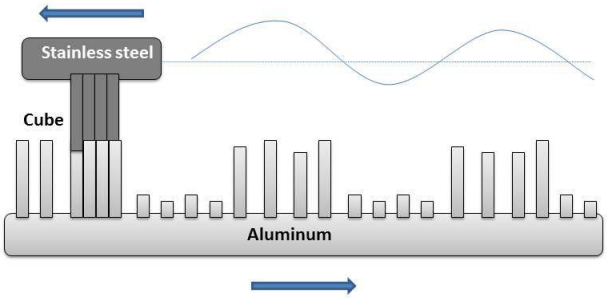

Figure 5. Mechanics of ultrasonically-induced wear reduction.

4. MODEL VALIDATION

4.1 Experimental set-up

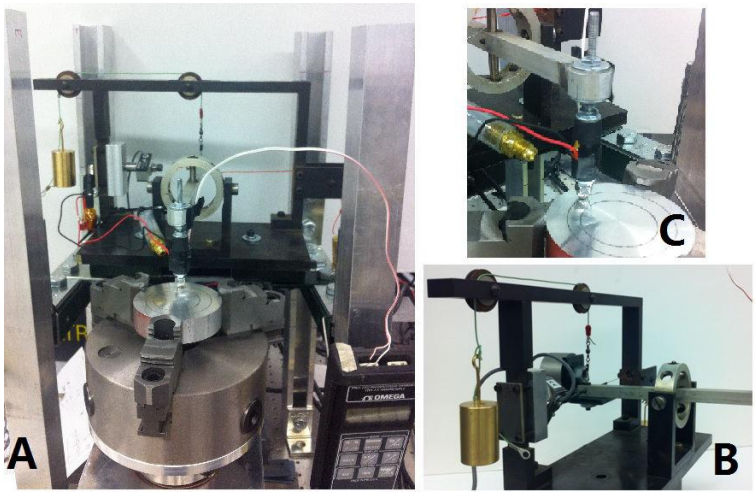

Figure 6. Experiment developed to investigate ultrasonic lubrication. A: modified pin-on-disc tribometer; B: gymbal assembly used to apply normal force; and C: disc sample and acorn nut connected to piezoelectric actuator.

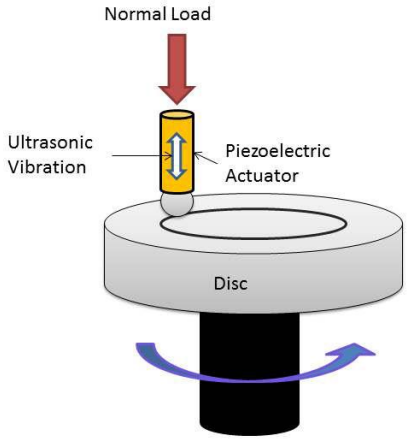

Figure 7. Schematic of modified pin-on-disc tribometer.

The experimental set-up used in this study is a modified pin-on-disc tribometer. A tribometer creates a contact between a still pin and a rotating disc for the purpose of studying the characteristics of friction and wear on the disc surface. The pin has been modified with the addition of a piezoelectric actuator and an acorn nut with a rounded end (Fig. 6). The actuator imparts ultrasonic vibrations to the rotating disc along the direction perpendicular to the disc. The tribometer is held by a lever which is part of a gymbal assembly that has been installed on the frame. Weights connected to the gymbal assembly apply normal loads to the interface. The normal force is measured before each test with a load sensor pad placed between the pin and the disc. The resistance of the sensor pad changes as a function of the applied force, resulting in a change of output voltage. The gymbal assembly is instrumented to measure friction forces using a load cell. The load cell is installed on

Table 1. Parameters utilized in the ultrasonic friction reduction tests.

Parameter	Value		
Linear speed (mm/s)	20.3	40.6	87
Running time (h)	4	2	0.93
Distance traveled by pin (m)	292.5		
Revolutions	1600		
Pin material	Stainless steel 316		
Disc material	Aluminum 2024		
Nominal normal force (N)	3		
Disc run out (mm)	$\pm$0.0286		
US frequency (kHz)	22		
US amplitude (μm)	2.5		
Nominal groove diameter (mm)	50		
Nominal temperature (°C)	21$\pm$1		
Nominal actuator temperature (°C)	31$\pm$1		
Environment	Laboratory air		
Sampling frequency (Hz)	400		

one side of the assembly frame and pretensioned horizontally by a weight on the other side. A schematic is shown in Fig. 7.

The piezoelectric actuator generates vibration of 2.5 μm at a frequency of 22 kHz. The temperature of the actuator can increase rapidly from the heat generated and accumulated during the test. To maintain even temperatures, air flow and a thermocouple are employed to cool down the actuator and monitor the temperature, respectively. The disc is 3 inches in diameter and held in place by a lathe chuck. The chuck, which is placed on a platform, is driven by a DC motor under it with adjustable rotating speeds.

4.2 Friction reduction validation

Two experiments were conducted on the modified tribometer to validate the "cube" model. Experiment 1 was conducted between stainless steel acorn nuts and aluminum discs at linear speeds of 20.3, 40.6, and 87 mm/s to investigate the relationship between friction reduction and sliding speeds. The distance traveled by the pin and the number of revolutions were kept constant by changing the duration of the test. For each speed, tests were conducted with and without ultrasonic vibrations. The remaining test parameters were fixed as shown in Table 1. Friction force was sampled at a frequency of 400 Hz and each sampling window was 2 seconds.

The mean value of the variation was calculated for each sampling window. All the values of friction forces are plotted against pin travel distance in Fig. 8. Different colors are used for different speeds, while dots represent friction values without ultrasonic vibrations, and "x" markers represent friction force values with ultrasonic vibrations. In both cases with and without ultrasonic vibrations, the friction force increases rapidly initially, reaches steady state after a certain travel distance, and remains at that level for the remainder of the test.

For all three speeds, the steady-state friction forces without ultrasonic vibrations are shown as red squares in Fig. 9. Based on the "cube" model, nominal dynamic friction F_t is equal to 0.91 N in this situation, and the relationship between overall friction and velocity is $F_f = 6.58v + 0.91$. Friction forces with ultrasonic vibrations are plotted as green diamonds in the figure. It can be seen that the model calculation matches the experimental data well at speeds of 40.8 mm/s and 87 mm/s, but with a bigger error at the lower speed of 20.4 mm/s. Figure 10 shows friction force within one ultrasonic vibration period for each speed. When the surfaces move towards each other, the relative motion pauses, and friction force is not reduced. This stage is called stick. When the surfaces move apart from each other, the relative motion continues, and the friction force is largely reduced.

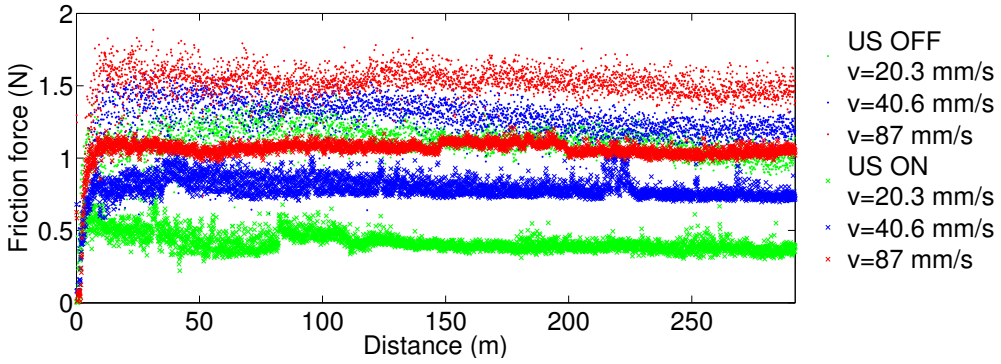

Figure 8. Friction forces with and without ultrasonic vibrations at various speeds.

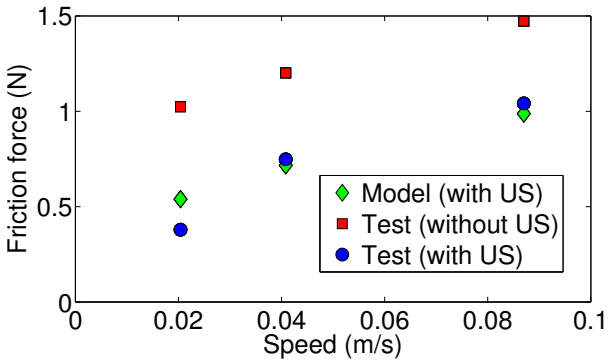

Figure 9. Comparison of experimental data and model calculation of friction forces.

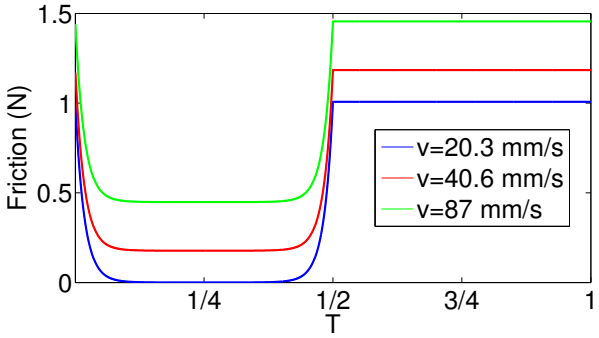

Figure 10. Friction force variation in one ultrasonic vibration cycle.

4.3 Wear reduction validation

Stainless steel acorn nuts and aluminum discs were tested for wear reduction for 900, 1600, and 1900 revolutions at a constant angular speed, which results in different pin travel distances, as shown Table 2. For each revolution,

Table 2. Parameters utilized in ultrasonic wear reduction tests.

Parameter	Value		
Running time (h)	1	1.68	2
Distance traveled by pin (m)	75.2	126.4	150.5
Revolutions	960	1600	1900
Linear speed (mm/s)	20.3		

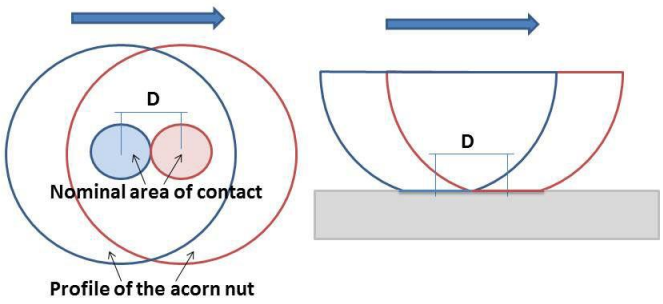

Figure 11. Schematic of wear rate calculation.

Table 3. Parameters used in model calculation.

Symbol	Meaning	Value
F_n	Normal force	3 N
E^*	Combined Young′s modulus	59.6 GPa
A_n	Nominal contact area	2.25 mm^2
R_q	RMS of asperity heights	6 μm
R_s	Summit radius of single asperity	1.5 μm
η	Areal density of asperities	4.7×10^{10} $/m^2$
Y_0	Yield strength of softer material	410 MPa

tests were conducted with and without ultrasonic vibrations. The remaining test parameters were kept the same as the ones from friction reduction experiments, shown in Table 1. Wear in these tests is abrasive due to the fact that stainless steel is harder than aluminum. This experiment is designed to investigate the relationship between abrasive wear reduction and the number of revolutions traveled by the pin relative to the disc.

An approach to quantify wear reduction is illustrated in Fig. 11. The geometry considered is that of the stainless steel acorn nut used in the experiment as it slides relative to the aluminum disc. Distance D can be calculated from the nominal area A_n as

$$D = \frac{4\sqrt{A_n}}{\pi}. \tag{24}$$

The value of A_n as well as other parameters utilized in modeling are listed in Table 3. The values of volume loss and wear rate are calculated and listed in Table 4. Volume losses of all tests are plotted in Fig. 12. It can be seen that the volume loss has a linear relationship with macroscopic speed both with and without ultrasonic vibrations. The cube model prediction and a comparison with the experimental data are listed in Table 5. It is shown that the model describes the wear reduction with errors smaller than 10%.

Table 4. Wear reduction data with and without ultrasonic vibrations.

Parameter	Value		
Revolutions	950	1600	1900
Volume loss without US (mm^3)	1.815	3.229	3.839
Wear rate without US (mm^3/m)	2.414×10^{-2}	2.554×10^{-2}	2.551×10^{-2}
Volume loss with US (mm^3)	1.134	1.745	2.094
Wear rate with US (mm^3/m)	1.509×10^{-2}	1.381×10^{-2}	1.392×10^{-2}
Wear reduction (%)	37.50	45.95	45.45

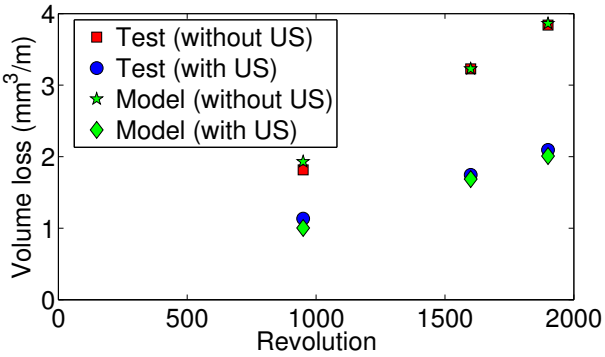

Figure 12. Volume loss with and without ultrasonic vibrations at various distances.

Table 5. Comparison of experimental data and model calculation of wear reduction.

Revolution	Wear rate (mm^3/m)					
	Without US			With US		
	test	model	error	test	model	error
900	2.414×10^{-2}	2.566×10^{-2}	6.3%	1.509×10^{-2}	1.355×10^{-2}	10.2%
1600	2.554×10^{-2}		0.47%	1.381×10^{-2}		1.89%
1900	2.551×10^{-2}		0.59%	1.392×10^{-2}		2.66%

5. CONCLUDING REMARKS

This paper presents an analytical cube model for ultrasonic friction and wear reduction. The overall friction force is considered as a sum of nominal dynamic friction and viscous friction. The nominal dynamic friction is solely related to the tangential deformation of contacting asperities. The amplitude of the ultrasonic vibrations creates a reduction of the nominal dynamic friction. Viscous friction is only dependent on the relative velocity between two surfaces. The velocity change caused by ultrasonic vibrations is responsible for the change of the viscous force. Therefore, the reduction of the overall friction force includes both nominal dynamic friction and viscous friction components. A model for abrasive wear reduction based on the cube concept is also proposed. A modified tribometer was designed and built. Two experiments were conducted and the data was utilized to validate the model. The model prediction matches the experimental data well with errors less than 10%.

ACKNOWLEDGMENTS

We wish to acknowledge the member organizations of the Smart Vehicle Concepts Center, a National Science Foundation Industry/University Cooperative Research Center (www.SmartVehicleCenter.org) established under NSF Grant IIP-1238286.

REFERENCES

[1] Bhushan, B., "Introduction to tribology," *John Wiley & Sons*, New York (2002).

[2] Bharadwaj, S. and Dapino, M. J., "Effect of load on active friction control using ultrasonic vibrations," *Proc. SPIE*, **7290**, 72900G (2009).

[3] Bharadwaj, S. and Dapino, M. J., "Friction control in automotive seat belt systems by piezoelectrically generated ultrasonic vibrations," *Proc. SPIE*, **7645**, 76450E (2010).

[4] Dong, S. and Dapino, M. J., "Piezoelectrically-induced ultrasonic lubrication by way of Poisson effect," *Proc. SPIE*, **8343L** (2012).

[5] Dong, S. and Dapino, M. J., "Elastic-plastic cube model for ultrasonic friction reduction via Poisson effect," *Ultrasonics*, **54**, 343-350 (2014).

[6] Dong, S. and Dapino, M. J., "Wear reduction through piezoelectrically-assisted ultrasonic lubrication," *Proc. ASME conference on SMASIS*, Snowbird, Utah, (2013).

[7] Dong, S. and Dapino, M. J., "Wear reduction through piezoelectrically-assisted ultrasonic lubrication," *Smart. Mater. Struct.* (Submitted).

[8] Uchino, K., "Piezoelectric ultrasonic motors: overview," *Smart. Mater. Struct.*, **7**, 273-285 (1998).

[9] Atherton, M., Mares, C., and Stolarski, T., "Some fundamental aspects of self-levitating sliding contact bearings and their practical implementations," *Proc. Inst. Mech. Eng. Part J: J. Eng. Tribol.*, **0**, 1-12 (2014).

[10] Severdenko, V., Klubovich, V., and Stepanenko, A., "Ultrasonic rolling and drawing of metals," *Consultants Bureau*, New York and London (1972).

[11] Littmann, W., Storck, H., and Wallaschek, J., "Sliding friction in the presence of ultrasonic oscillations: superposition of longitudinal oscillations," *Arch. Appl. Mech.*, **71,** 549-554 (2001).

[12] Littmann, W., Storck, H., and Wallaschek, J., "Reduction in friction using piezoelectrically excited ultrasonic vibrations," *Proc. SPIE*, **4331** (2001).

[13] Kumar, V. and Hutchings, I. "Reduction of the sliding friction of metals by the application of longitudinal or transverse ultrasonic vibration," *Tribol. Int.*, **37**, 833-840 (2004).

[14] Popov, V., Starcevic, J., and Filippov, A., "Influence of ultrasonic in-plane oscillations on static and sliding friction and intrinsic length scale of dry friction processes," *Tribol. Lett.*, **39**, 25-30 (2010).

[15] Chowdhury, M. and Helali, M., "The effect of frequency of vibration and humidity on the wear rate," *Wear*, **262**, 198-203 (2007).

[16] Bryant, M., Tewari, A., and York, D., "Effect of micro (rocking) vibrations and surface waviness on wear and wear debris," *Wear*, **216**, 60-69 (1998).

[17] Bryant, M. and York, D., "Measurements and correlations of slider vibrations and wear," *J. Tribol.*, **122**, 374-380 (2000).

[18] Goto, H., Ashida, M., and Terauchi, Y., "Effect of ultrasonic vibration on the wear characteristics of a carbon steel: analysis of the wear mechanism," *Wear*, **94**, 13-27 (1984).

[19] Goto, H., Ashida, M., and Terauchi, Y., "Wear behaviour of a carbon steel subjected to an ultrasonic vibration effect superimposed on a static contact load," *Wear*, **110**, 169-181 (1986).

[20] Polycarpou, A. A., and Etsion, I.,"Analytical approximations in modeling contacting rough surfaces," *ASME J. Tribol.*, **109**, 257-263 (1999).

[21] Shi, X., and Polycarpou, A. A., "Measurement and modeling of normal contact stiffness and contact damping at the meso scale," *ASME J. Tribol.*, **127**, 52-60 (2005).

[22] Olsson, H., Astrom, K., Canudas de Wit, C., Gafvert, M., and Lischinsky, P., "Friction models and friction compensation," *Eur. J. Control*, **4**, 176-195 (1998).